

10-14-2017


VUV Optical Properties of Rare Earth Doped YPO₄ Prepared by Different Routes

Zachary Way

Maxwell K. Wallace

Anthony L. Diaz

Follow this and additional works at: <https://digitalcommons.cwu.edu/cotsfac>

 Part of the [Chemistry Commons](#)



VUV Optical Properties of Rare Earth Doped YPO₄ Prepared by Different Routes

Zachary Way, Maxwell K. Wallace, and Anthony L. Diaz²

Department of Chemistry, Central Washington University, Ellensburg, Washington 98926, USA

The optical properties of nanocrystalline YPO₄:Ln³⁺ (Ln = Eu, Sm, Tb) prepared via co-precipitation are compared to larger crystallites of YPO₄:Ln³⁺ prepared via traditional solid state reaction. In larger crystals (~330 nm) a distinct peak is observed at 150 nm in the excitation spectra, the intensity of which decreases markedly in smaller crystals (~20 nm). Using excitation and reflectance spectroscopy, host-to-activator energy transfer efficiencies were calculated for Y_{1-x}PO₄:Ln³⁺ (0.01 ≤ x ≤ 0.10). From the transfer efficiency data, we estimate that trapping by Eu³⁺ and Sm³⁺ is at least five times more efficient than trapping by Tb³⁺ for excitation at the band edge. The fraction of energy lost to the surface or grain boundaries for excitation at 150 nm and 138 nm is also estimated. We propose that in the samples prepared via co-precipitation, an amorphous phase forms at grain boundaries that is responsible for the loss of efficiency under 150 nm excitation.

© The Author(s) 2017. Published by ECS. This is an open access article distributed under the terms of the Creative Commons Attribution 4.0 License (CC BY, <http://creativecommons.org/licenses/by/4.0/>), which permits unrestricted reuse of the work in any medium, provided the original work is properly cited. [DOI: 10.1149/2.0201801jss] All rights reserved.



Manuscript submitted July 24, 2017; revised manuscript received September 25, 2017. Published October 14, 2017. *This paper is part of the JSS Focus Issue on Visible and Infrared Phosphor Research and Applications.*

Rare-earth doped YPO₄ has been studied extensively, both for potential technological applications and in more fundamental investigations of electron transport and trapping processes.¹⁻⁴ Nakazawa reported on the vacuum ultraviolet (VUV) spectroscopy of Ln³⁺ doped microcrystalline YPO₄,⁴ and assigned excitations due to host, 4f–5d, and charge transfer transitions for all of the lanthanides (except Pm and Lu). Additional studies of YPO₄ include one by Lai et al. that described a precipitation route to ~20 nm YPO₄:Eu³⁺, but only the UV optical properties are discussed.⁵ Di et al. have compared the VUV optical properties of YPO₄:Tb³⁺ prepared via solid state reaction and co-precipitation.⁶ However, unlike in the work presented here, the high calcination temperatures applied to the co-precipitated samples led to materials that were similar in size to solid state samples but with improved morphology. Van Pieterse et al. obtained high-resolution excitation spectra of YPO₄ doped with both light⁷ and heavy⁸ lanthanides at 6 K. They assigned spectral features and compared the experimentally observed spectra with energy level calculations for the 4fⁿ–15d¹ states. Makhov et al. investigated the optical properties of YPO₄:Nd³⁺ under VUV synchrotron radiation over a temperature range of 9–300 K. Their work included the assignment of various host-sensitized excitation mechanisms that will be discussed more later.⁹ Several groups have also reported on the optical properties of double-doped YPO₄.¹⁰⁻¹² Much of that work was interpreted in the context of the lanthanide energy level scheme for YPO₄ reported by Bos et al.¹³ and Dorenbos and Bos,¹⁴ in which the Ln²⁺ and Ln³⁺ ground state energies are placed relative to the host valence and conduction bands. Of interest to the current study is the observation that the excitation spectra of some lanthanides (particularly Sm, Eu, Gd and Tm) contain a distinct, intense peak for excitation right at the band edge of YPO₄ (~150 nm). Since the focus of prior work was on assigning peaks in the excitation spectra, the authors generally make little comment on this somewhat unusual feature. However, understanding the origin of this efficient excitation may help provide guidance in the continued development of more efficient optical materials. Here we report on the VUV optical properties of YPO₄:Ln³⁺ prepared by solid state reaction and compare the results to nanocrystalline YPO₄:Ln³⁺ prepared via co-precipitation, in which we see a dramatic decrease in the intensity of the peak at 150 nm.

When a doped luminescent material is excited with energies greater than the host bandgap, an electron-hole (e-h) pair is created in the host that must be captured by the dopant for luminescence to occur. The efficiency of this capture is referred to as the transfer efficiency, η_t . It

has been shown that excitation and reflectance spectroscopy can, in some cases, be used to estimate the transfer efficiency in a material under host-sensitized (VUV) excitation. The data can be modeled to determine a relative e-h pair capture efficiency, and may also be used to estimate the degree of surface loss in nanocrystalline phosphors.¹⁵⁻¹⁷ In what follows we apply this approach to the study of YPO₄:Ln³⁺. The goal is to develop the structure–property relationships that govern efficient host-sensitized luminescence, by developing quantitative tools to evaluate these processes. We are also interested in comparing our quantitative work to previously developed kinetic models.

Experimental

Larger crystals (~330 nm, see below) of Y_{1-x}PO₄:Ln³⁺ were synthesized by grinding stoichiometric amounts of Y₂O₃, (NH₄)₂HPO₄, and rare earth oxide and firing at 1300°C for 8 hours. Nanocrystalline Y_{1-x}PO₄:Ln³⁺ samples were synthesized according to the method of Lai et al.⁵ Stoichiometric amounts of pure Y₂O₃ and Eu₂O₃ were dissolved in a HNO₃ solution. An appropriate volume of (NH₄)₂HPO₄ aqueous solution was then added and the pH was adjusted to 2 with ammonia. The solution was stirred for 2 hours at 50°C. The precipitate was separated using vacuum filtration and the resulting material was dried at 80°C. The dried precipitate was fired at 900°C for 3 hours. In the original report of Lai et al., Li₂CO₃ was added during the precipitation step and was proposed to act as a flux during firing. However, to reduce the number of variables in the current study, our samples were prepared without the Li₂CO₃. We did not observe any differences when the Li₂CO₃ was left out.

X-ray data were obtained with a Rigaku Miniflex 600 automated powder X-ray diffractometer. Scanning Electron Microscopy images were provided by the CAMCOR facility at the University of Oregon using a Zeiss Ultra-55. For spectroscopic measurements, the excitation source was composed of a 30 W D₂ lamp and VUV monochromator (ARC VM–502). The VUV monochromator uses a 1200 grooves/mm grating with a resolution of 0.4 nm or better, although our step size was 0.5 nm. The lamp, sample chamber, and excitation monochromator are pumped down to ~3 × 10⁻⁵ mbar using a dry diaphragm / turbo pump station (Pfeiffer Vacuum). For emission, a standard UV / vis monochromator (ARC SP–150) and photomultiplier tube (PMT) were used. For reflectance measurements, a VUV–PMT is used. Reflectance spectra were corrected using MgF₂, excitation spectra were corrected using a sodium salicylate standard, and emission spectra were corrected using a NIST calibrated standard lamp. For all samples, reflectance spectra were measured with and without a blocking

²E-mail: diaza@cwu.edu

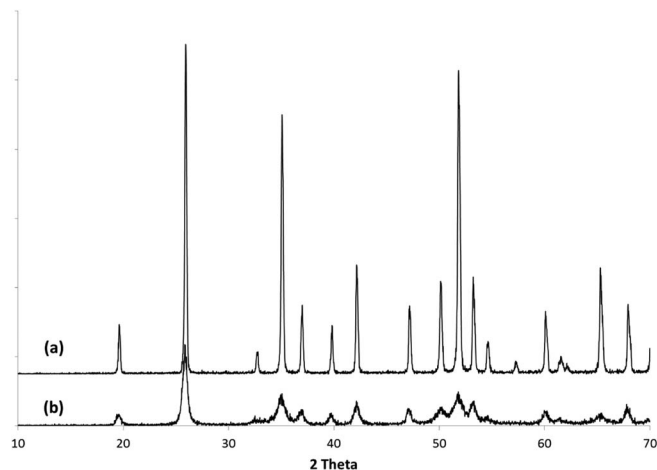


Figure 1. Powder X-ray diffraction patterns of $\text{YPO}_4:\text{Eu}^{3+}$ (a) prepared by traditional solid-state methods and fired at 1300°C and (b) prepared via co-precipitation and fired at 900°C .

filter in order to subtract sample emission out of the raw reflectance data.

Results and Discussion

All samples were found to be phase pure by X-ray diffraction. Representative powder XRD data are shown in Figure 1. These exhibit the expected line broadening at smaller particle sizes. The particle diameters estimated using the Williamson - Hall method are found to be approximately 20 nm for the samples prepared via co-precipitation and approximately 330 nm for samples prepared via grind and firing. Scanning electron microscope images are shown in Figure 2. Both preparations result in polycrystalline agglomerates. The images allow an estimate of the particle size of the samples prepared by grind and firing (250–300 nm), whereas individual crystallites cannot be distinguished for the samples prepared by co-precipitation.

Before discussing the optical properties of the various doped samples, it is useful to present the absorption spectra of the undoped compounds. These spectra (as 1-R) are shown in Figure 3 for YPO_4 prepared by both methods. Two important features are worth noting. First, the sample prepared by solid state methods exhibits a distinct onset of band edge absorption at about 148 nm. In the co-precipitation sample, this absorption is less distinct, instead appearing as a broad feature with absorption to longer wavelengths. We believe that the most reasonable interpretation for the difference in absorption is the presence of an amorphous phase at the grain boundaries of the particles prepared via co-precipitation. Those samples also exhibit considerably higher background, presumably due to a difference in the light scattering properties of the smaller grains. We associate the small peak at 207 nm with impurities. We note also that we collected IR spectra of both samples, but we saw essentially no difference between them.

Emission spectra of $\text{YPO}_4:\text{Eu}$ prepared both ways are shown in Figure 4. Excitation is via the host at 150 nm. The spectra exhibit characteristic $^5\text{D}_0 \rightarrow ^7\text{F}_1$ and $^5\text{D}_0 \rightarrow ^7\text{F}_2$ transitions at 593 nm and 615 nm, respectively, and are comparable to what has been reported previously for this material.^{1,6} The relatively high intensity of the $^5\text{D}_0 \rightarrow ^7\text{F}_1$ transition is indicative of Eu^{3+} occupying a site with inversion symmetry, consistent with the Y site symmetry in YPO_4 .¹⁸ We observe no systematic change in the ratio of these two peaks with Eu concentration. However, we do observe a slight increase in the red/orange ratio in the smaller crystallites. An increase in the relative amount of $^5\text{D}_0 \rightarrow ^7\text{F}_2$ emission implies that the inversion symmetry is being relaxed, which is likely the result of lower crystallinity in the 20 nm material. Spectra were collected up to 10 mol% Eu, and it appears that quenching may begin to set in around 10 mol%.

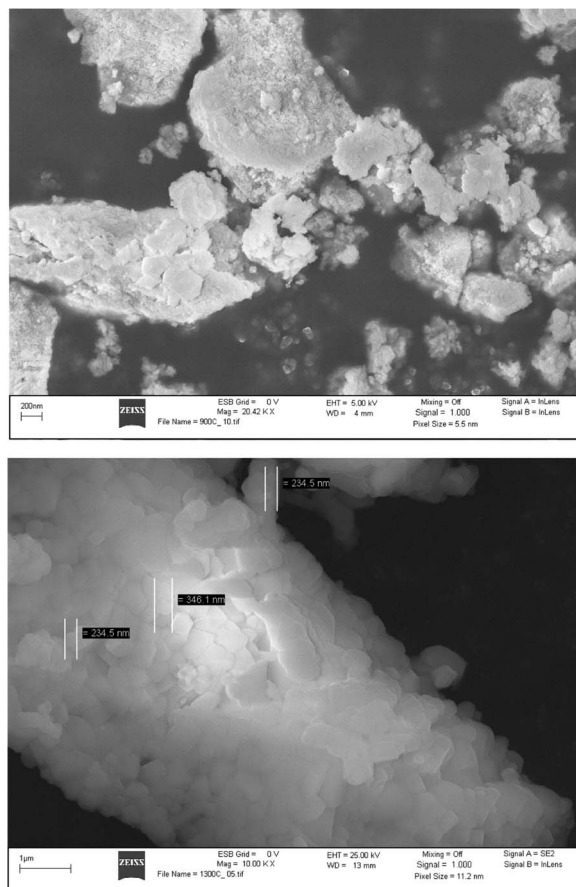


Figure 2. SEM images of $\text{YPO}_4:\text{Eu}^{3+}$ prepared via co-precipitation (above, scale bar = 200 nm) and prepared by traditional solid-state methods (below, scale bar = $1\ \mu\text{m}$).

Representative excitation spectra are shown in Figure 5 for $\text{YPO}_4:\text{Eu}$ prepared both ways. Features at wavelengths shorter than 150 nm are associated with excitation via the YPO_4 host, while features at longer wavelengths are due to Eu charge transfer (CT) excitation. There are several curious features that appear in the excitation spectra. Most notable is a sharp peak at ~ 150 nm that decreases dramatically at small crystallite sizes. This is observed regardless of Eu concentration. Secondly, the CT band appears to exhibit two broad peaks, rather than one.

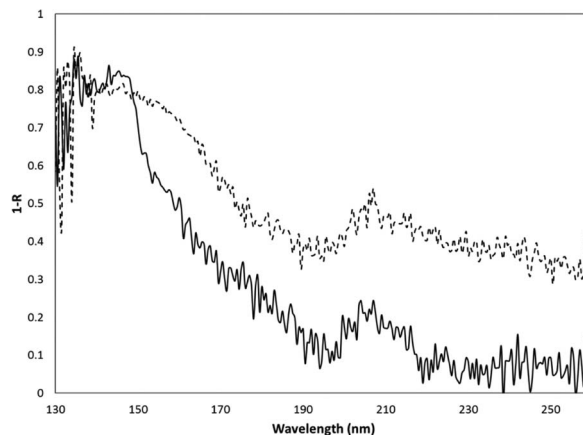


Figure 3. Absorption spectra (as 1-R) of YPO_4 prepared by traditional solid-state methods (solid line) and via co-precipitation (dashed line).

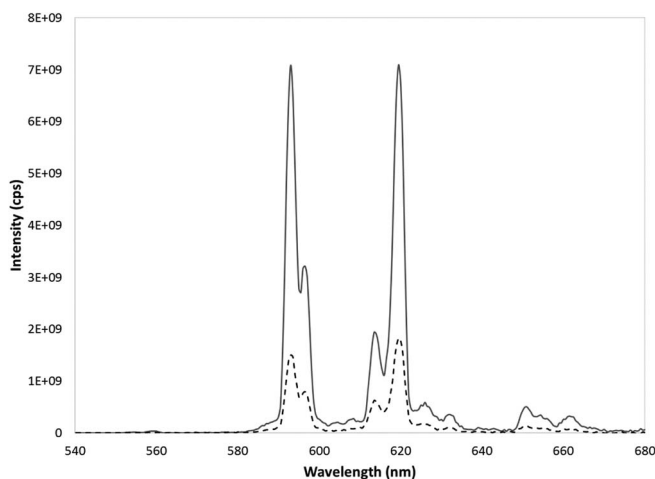


Figure 4. Emission spectra of $\text{Y}_{0.95}\text{PO}_4:\text{Eu}_{0.05}$ prepared via solid state methods (solid line) and via co-precipitation (dashed line). $\lambda_{\text{ex}} = 150$ nm.

The unusual shape of the CT band is not apparent in reports that discuss only UV excitation of $\text{YPO}_4:\text{Eu}$ ^{1,5} because typical UV instruments do not provide significant excitation intensity below ~ 250 nm. It is our opinion that the position of the CT is not correctly determined in that case. In the reports of VUV excitation^{3,4,7} the spectra more closely resemble what we report here (a broad, asymmetric feature at ~ 225 nm). However, the asymmetric nature of the CT excitation is not commented on. The shape of the excitation suggests the possibility of two distinct Eu^{3+} sites. However, there is only a single Y site in YPO_4 ¹⁸ and we see no differences in the line ratios of emission spectra as we vary the excitation across this band, which suggests that there is only one type of Eu^{3+} . We also note that there is little change in the shape (although not the intensity) of the CT band with concentration. We might speculate that the two peaks represent charge transfer from different O atoms in the lattice, given that in YPO_4 there are two sets of four O atoms around the Y site at 2.39 and 2.57 Å. However, we have not seen this type of argument presented in the literature, and excitation spectra of the other dopants studied suggest only one type of activator site. Thus at this point we can propose no definitive explanation for the shape of the Eu^{3+} CT band, and in what follows we make the assumption that there is only a single Eu^{3+} site. Finally, we observe a change in the shape of the CT band in the co-precipitated samples, in which there is a decrease in intensity on the short wave-

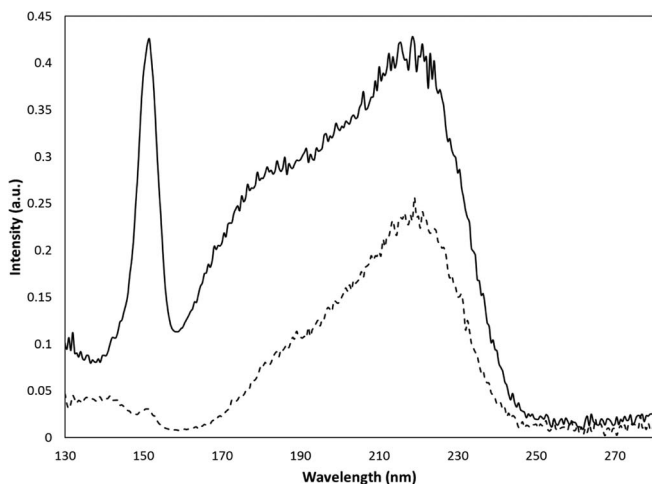


Figure 5. Excitation spectra of $\text{Y}_{0.99}\text{PO}_4:\text{Eu}_{0.01}$ prepared by traditional solid-state methods (solid line) and via co-precipitation (dashed line). $\lambda_{\text{em}} = 592$ nm.

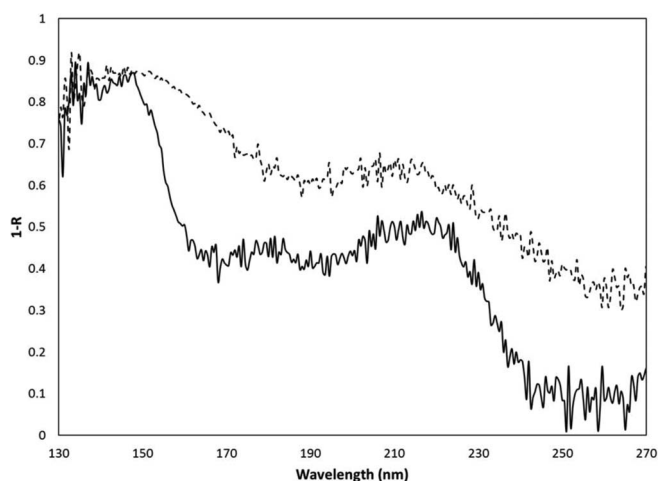


Figure 6. Absorption spectra (as 1-R) of $\text{Y}_{0.99}\text{PO}_4:\text{Eu}_{0.01}$ prepared by traditional solid-state methods (solid line) and via co-precipitation (dashed line).

length side of the band (170–200 nm). An explanation for this may be provided by the absorption data.

Absorption, as 1-R, for $\text{YPO}_4:\text{Eu}$ is shown in Figure 6 for both preparations. Absorption spectra are generally much noisier than emission and excitation spectra. This is due to the fact that there is lower signal than in the other two measurements, compounded by the fact that the final spectra are a combination of three measurements, generated as (with filter) – (without filter) then divided by the reflectance of MgF_2 . In the solid state samples, the band edge is distinguishable at ~ 150 nm, with CT absorption taking place between 170 and 230 nm. The CT absorption mimics the double peak seen in excitation spectra. In the co-precipitation samples, the distinct absorption at the band edge is somewhat washed out by the broad absorption feature that is seen in the undoped samples. In both cases, we observe that CT absorption increases with Eu concentration. We believe that the change in the shape of the CT band in the co-precipitation samples is due to interference from the phase that is causing the long absorption tail after the band edge. This phase blocks excitation of Eu in the 170–200 nm window and thus reduces the observed excitation intensity.

Similar optical data sets were obtained for $\text{YPO}_4:\text{Sm}^{3+}$ prepared both ways. Representative emission data are shown in Figure 7, excitation in Figure 8, and absorption as 1-R in Figure 9. Unlike with Eu^{3+} , we observe that Sm^{3+} exhibits significant concentration quenching

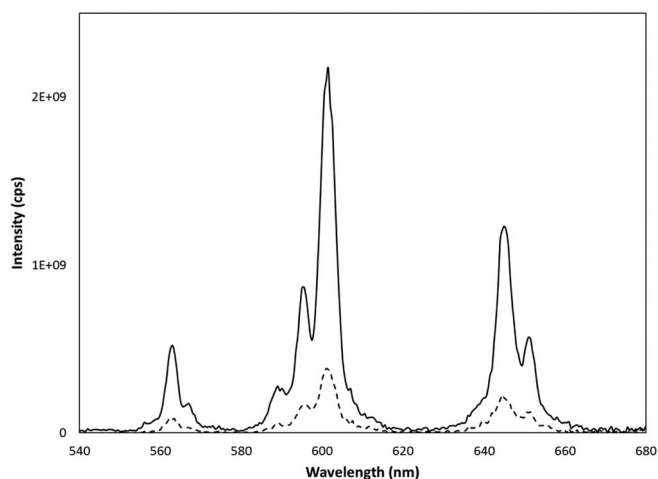


Figure 7. Emission spectra of $\text{Y}_{0.95}\text{PO}_4:\text{Sm}_{0.05}$ prepared via solid state methods (solid line) and via co-precipitation (dashed line). $\lambda_{\text{ex}} = 150$ nm.

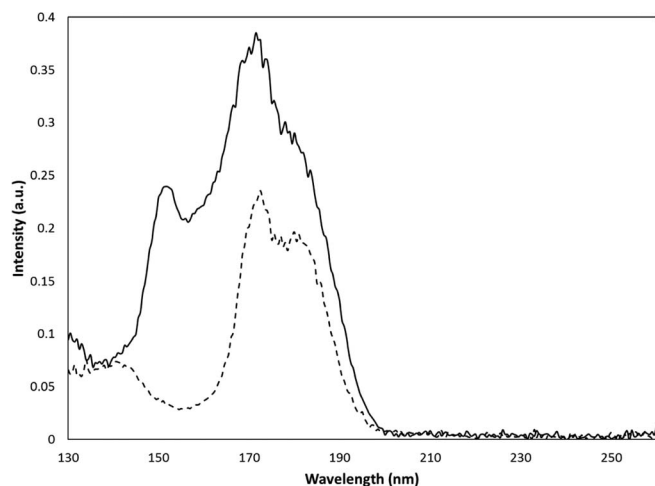


Figure 8. Excitation spectra of $Y_{0.99}PO_4:Sm_{0.01}$ prepared by traditional solid-state methods (solid line) and via co-precipitation (dashed line). $\lambda_{em} = 601$ nm.

after 1 mol%. In the excitation spectra, a distinct peak appears at 150 nm in the solid state samples that again decreases substantially in the co-precipitation samples. Two additional peaks at 175 nm and 180 nm have been assigned to $4f - 5d$ and CT transitions, respectively.⁴ In the absorption data we again observe that the band edge can be distinguished in the solid state samples, but this feature is washed out by a broad absorption in the co-precipitation samples.

Optical data sets were also obtained for $YPO_4:Tb^{3+}$ prepared both ways. Representative emission data are shown in Figure 10, excitation in Figure 11, and absorption as 1-R in Figure 12. Tb^{3+} does not exhibit significant concentration quenching up to 10 mol%. In the excitation spectra, the distinct peak at 150 nm in the solid state samples is still present, though to a lesser degree than is observed with Eu and Sm. This peak again decreases substantially in the co-precipitation samples. Additional peaks at wavelengths longer than 160 nm have been assigned to $4f - 5d$ transitions.^{4,6} In the absorption data we again observe that the band edge feature is washed out by the broad absorption in the co-precipitation samples, although the difference is less obvious than with Eu and Sm. Although the absorption data are very noisy and it can be difficult to distinguish some features in the spectra, we believe it is still instructive to consider the results, particularly when it comes to estimating host-to-activator transfer efficiencies as is discussed later.

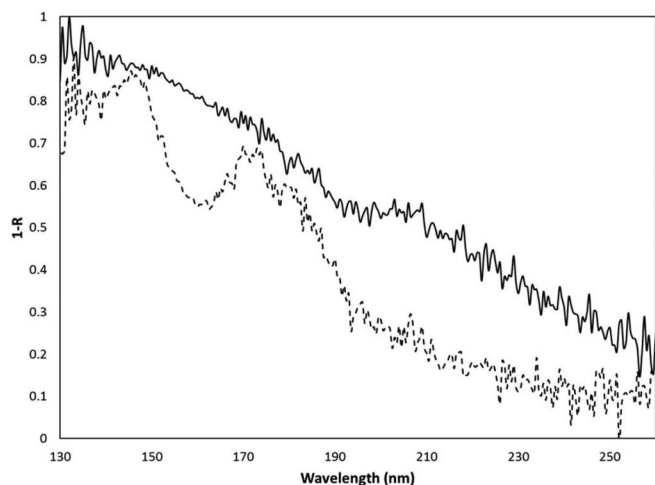


Figure 9. Absorption spectra (as 1-R) of $Y_{0.99}PO_4:Sm_{0.01}$ prepared by traditional solid-state methods (solid line) and via co-precipitation (dashed line).

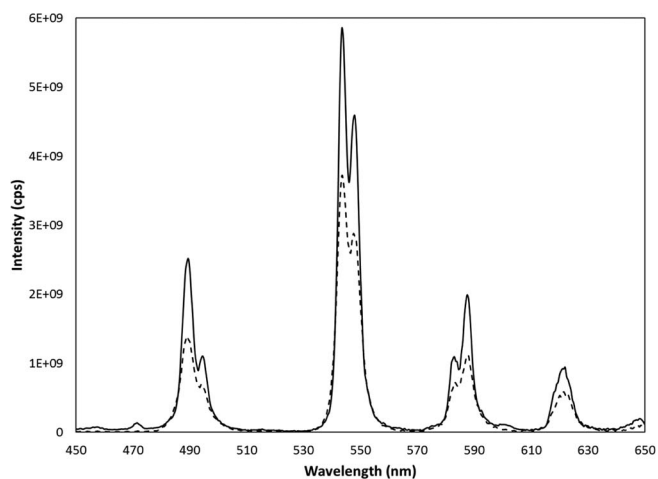


Figure 10. Emission spectra of $Y_{0.95}PO_4:Tb_{0.05}$ prepared via solid state methods (solid line) and via co-precipitation (dashed line). $\lambda_{ex} = 150$ nm.

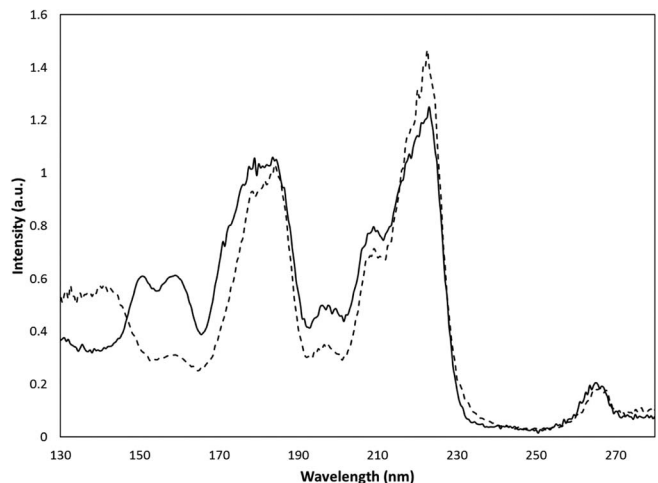


Figure 11. Excitation spectra of $Y_{0.95}PO_4:Tb_{0.01}$ prepared by traditional solid-state methods (solid line) and via co-precipitation (dashed line). $\lambda_{em} = 543$ nm.

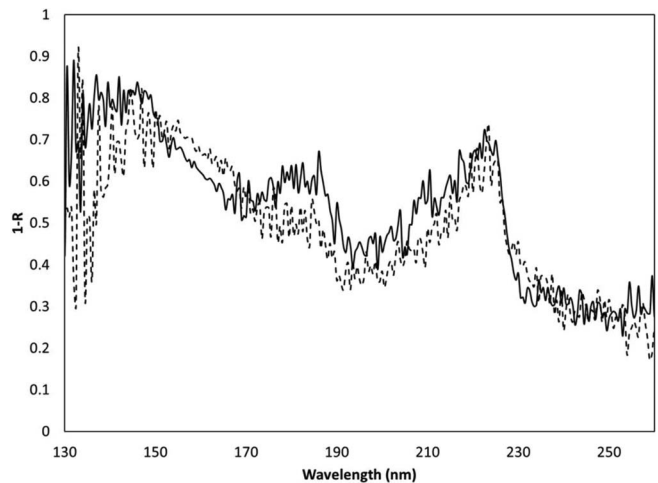


Figure 12. Absorption spectra (as 1-R) of $Y_{0.99}PO_4:Tb_{0.01}$ prepared by traditional solid-state methods (solid line) and via co-precipitation (dashed line).

In the excitation spectra, the sharp peak at 150 nm can reasonably be assigned to excitation at the band edge of the YPO₄ host. It corresponds almost exactly with the observed band edge absorption and is in the same place for all dopants. Nakazawa and Shiga³ assigned this feature to phosphate absorption. We note, however, that density of states calculations indicate that the top of the valence band is comprised primarily of O 2p states, while the bottom of the conduction band is primarily Y 4d,¹⁹ suggesting that band edge excitation would involve these states rather than PO₄³⁻ states. In the low temperature work of Makhov et al., they proposed a bandgap of 9.4 eV (~132 nm) based on lifetime measurements of YPO₄:Nd³⁺ emission under host versus direct excitation.⁹ They also observed self-trapped exciton (STE) emission at 430 nm, with the excitation spectrum of this emission indicating STE formation at about 8.4 eV (~147 nm). In YPO₄:Eu³⁺, van Pieterse et al. assigned the peak at ~150 nm to 4f → 5d transitions.⁷ This suggests the possibility that the STE energy and the Eu³⁺ 4f → 5d energy match very closely. Interestingly, we find that the intensity of this peak is somewhat activator dependent, as was observed previously (although not commented on) by Nakazawa.⁴ Bos et al. published the energy level scheme for lanthanides in YPO₄ which was arrived at using a semi-empirical method.¹³ Thermoluminescence experiments confirm that the scheme provides a reasonable estimate of the location of Ln²⁺ and Ln³⁺ ground states relative to host states.¹⁴ Using this scheme we note that the sharp feature at 150 nm appears most pronounced for cases in which the Ln³⁺ ground state energy is lower than (or very close to) the valence band energy (i.e. Eu³⁺, Sm³⁺, Tm³⁺), while this feature is less prominent or not observed when the Ln³⁺ ground state energy is notably greater than the valence band edge (i.e. Tb³⁺, Dy³⁺). Thus it is possible that the enhanced excitation efficiency is due to more efficient capture of the electron-hole pair when activator ground states are in the valence band, perhaps via resonant capture of a self-trapped exciton formed from excitation at the band edge. Certainly more systematic work needs to be done to clarify this phenomenon, and we only mention it here as a general observation. It may also point to the additional utility of developing energy level schemes using Dorenbos' method. Based on our excitation spectra, at small particle sizes either surface states or an amorphous interface phase are present that absorb or trap this excitation energy before it can be transferred to the dopant. Note that absorption spectra for both particle sizes generally show a relatively high and uniform absorption for wavelengths shorter than the band edge.

Recently, several studies have been published that attempt to quantify the efficiency of energy transfer to a dopant under host excitation, using excitation and reflectance spectra.^{15–17,20} Here, we are interested in comparing transfer efficiency for the two preparative methods, as well as quantifying the diversion of energy at 150 nm in the coprecipitation samples.

The calculation of the transfer efficiency begins by taking the quantum efficiency of host excitation, η_{host} , to be:

$$\eta_{host} = \eta_t \cdot \eta_{act} \quad [1]$$

where η_{act} is the quantum efficiency of the activator and η_t is the host-to-activator transfer efficiency. This expression can be rewritten by substituting the efficiency terms with their representative emitted and absorbed photon fluxes, Φ :

$$\frac{\Phi_{em}^{host}}{\Phi_{abs}^{host}} = \eta_t \cdot \frac{\Phi_{em}^{act}}{\Phi_{abs}^{act}} \quad [2]$$

In this notation, the subscript denotes absorbed or emitted fluxes while the superscript denotes if absorption or excitation is via the host or directly via the activator (i.e. Φ_{em}^{host} refers to the amount of activator emission observed via host-lattice excitation). Equation 2 can be rearranged to

$$\eta_t = \frac{\Phi_{em}^{host}}{\Phi_{act}^{act}} \cdot \frac{\Phi_{abs}^{act}}{\Phi_{abs}^{host}} \quad [3]$$

The first ratio in Equation 3 is taken from excitation spectra. This gives the relative intensities of activator emission under host and di-

rect excitation. We find that the shape of the excitation spectra are insensitive to the choice of emission wavelength (i.e. the ratios obtained for Equation 3 are the same), and the most intense peak in the emission spectrum of each dopant was used to collect excitation spectra. The second ratio is taken from absorption data (as 1-R) and is the relative ratio of activator and host absorption. A more thorough discussion of the development and assumptions regarding this expression is provided in previous publications.^{15,16,20,21} In spite of some obvious shortcomings, this type of analysis has proven to provide interesting insight into the e-h transport and trapping properties of a number of luminescent systems. It has the advantage of using ratios taken from the same spectrum, while avoiding the need for trying to measure absolute quantum efficiencies.

Excitation and absorption data were obtained for Ln³⁺ concentrations of 1, 2, 5 and 10 mol%, and flux values to use in Equation 3 were obtained from these spectra. For the activator flux terms (Φ_{em}^{act} and Φ_{abs}^{act}), we chose the wavelength of the most intense peak in the excitation spectrum for each dopant (220 nm for Eu³⁺, 172 nm for Sm³⁺, and 222 nm for Tb³⁺). For the host terms (Φ_{em}^{host} and Φ_{abs}^{host}) we used intensities at 150 nm as well as 138 nm. That is, the transfer efficiency was calculated for excitation at each of these wavelengths separately. This allows us to compare energy transfer from the unusual excitation at 150 nm to energy transfer from higher energies that appear to be less affected by the preparation method. In addition, excitation at 138 nm versus 150 nm is expected to result in different types of processes within the host: 138 nm is sufficient energy to produce mobile e-h pairs, whereas excitation at 150 creates STE's. Dorenbos previously referred to this as the "mobility gap", and suggested that mobile e-h pairs are created when the excitation energy is at least 8% greater than the absorption edge.²²

By way of an example calculation of transfer efficiency, consider the excitation and absorption data for YPO₄:Eu³⁺ prepared by solid state methods, presented in Figures 5 and 6. From the excitation spectra we obtain values of $\Phi_{em}^{host} = 0.42$ at 150 nm and $\Phi_{em}^{act} = 0.41$ at 220 nm. From the absorption spectra we obtain values of $\Phi_{abs}^{host} = 0.85$ at 150 nm and $\Phi_{abs}^{act} = 0.50$ at 220 nm. Plugging these into Equation 3 results in $\eta_t = 0.59$. That is, 59% of absorbed energy is trapped by Eu³⁺ at a concentration of 1 mol%. Complete data sets and flux values are available on request. Here, we report the final results. Transfer efficiencies plotted versus activator concentration, as well as reciprocal plots ($1/\eta_t$ vs $1/[\text{Ln}^{3+}]$), are provided in Figures 13–15 for both preparation methods. Concentrations have been converted to Ln³⁺/cm³ using the mole% and the structure of YPO₄.¹⁸ The η_t calculation was performed for host excitation at both 138 and 150 nm. As expected, η_t increases with Ln³⁺ concentration as trapping of an e-h pair becomes more likely. Under 138 nm excitation, the transfer efficiency is relatively insensitive to the preparation method. Under 150 nm excitation e-h trapping is much more efficient for the large particles, consistent with the excitation spectra discussed above.

These data can be modeled using first-order competition kinetics where, for excitation energies just greater than the bandgap, the transfer efficiency is given by:^{16,22}

$$\eta_t = \frac{\alpha N}{\alpha N + \beta} \times S_{loss} \quad [4]$$

The term α is the rate constant for trapping by activators, N is the activator concentration, and β is the overall rate of transfer to killers. Therefore, αN is the rate of transfer to activators (rate constant \times concentration) and the transfer efficiency is the ratio of the rate of transfer to activators to the total trapping rate (the sum of rates to activators plus killers). Killer concentration is assumed to be a feature of the host and not affected by the activator concentration. The term S_{loss} represents energy lost to the particle surface, where $S_{loss} = 1$ corresponds to no surface losses. Values of S_{loss} less than 1 represent the fraction of the e-h pairs that are available for transport and trapping by a dopant (i.e. if $S_{loss} = 0.8$, then 80% of excitation energy is available for trapping). In this treatment, S_{loss} is assumed to be a constant. This approach was used previously to quantify surface loss effects in nanocrystalline YBO₃:Eu³⁺ and Y₂O₃:Eu³⁺.^{16,17} It is

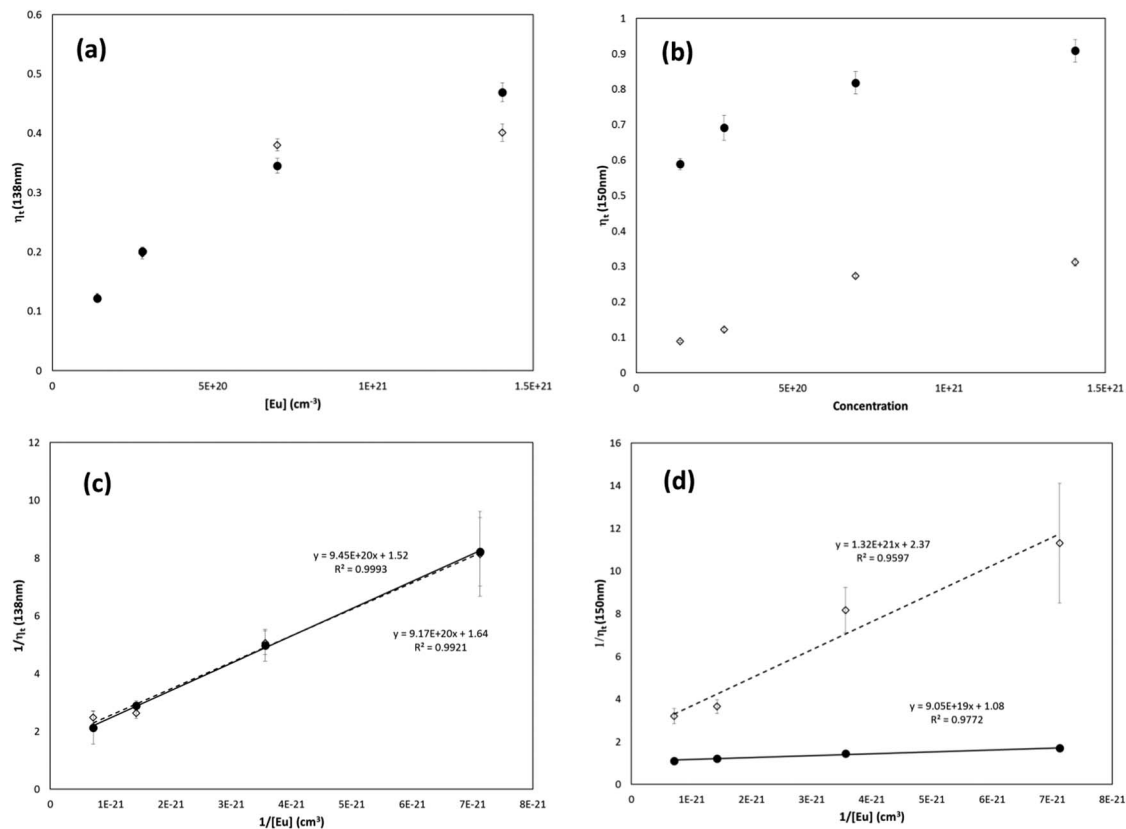


Figure 13. Transfer efficiency versus Eu³⁺ concentration in YPO₄:Eu for excitation at (a) 138 nm and (b) 150 nm. Reciprocal plots of these data are in (c) and (d). Solid circles are for samples prepared by solid state reaction, while open diamonds were prepared via co-precipitation.

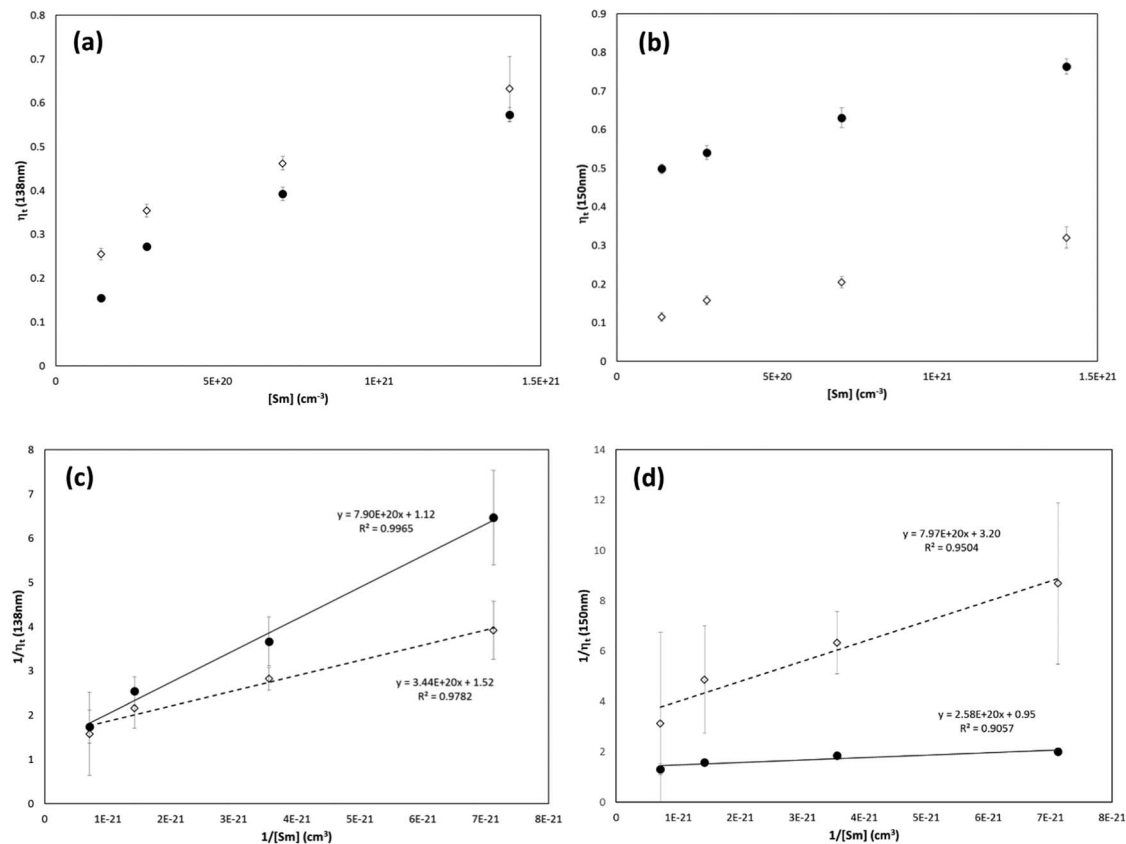


Figure 14. Transfer efficiency versus Sm³⁺ concentration in YPO₄:Sm for excitation at (a) 138 nm and (b) 150 nm. Reciprocal plots of these data are in (c) and (d). Solid circles are for samples prepared by solid state reaction, while open diamonds were prepared via co-precipitation.

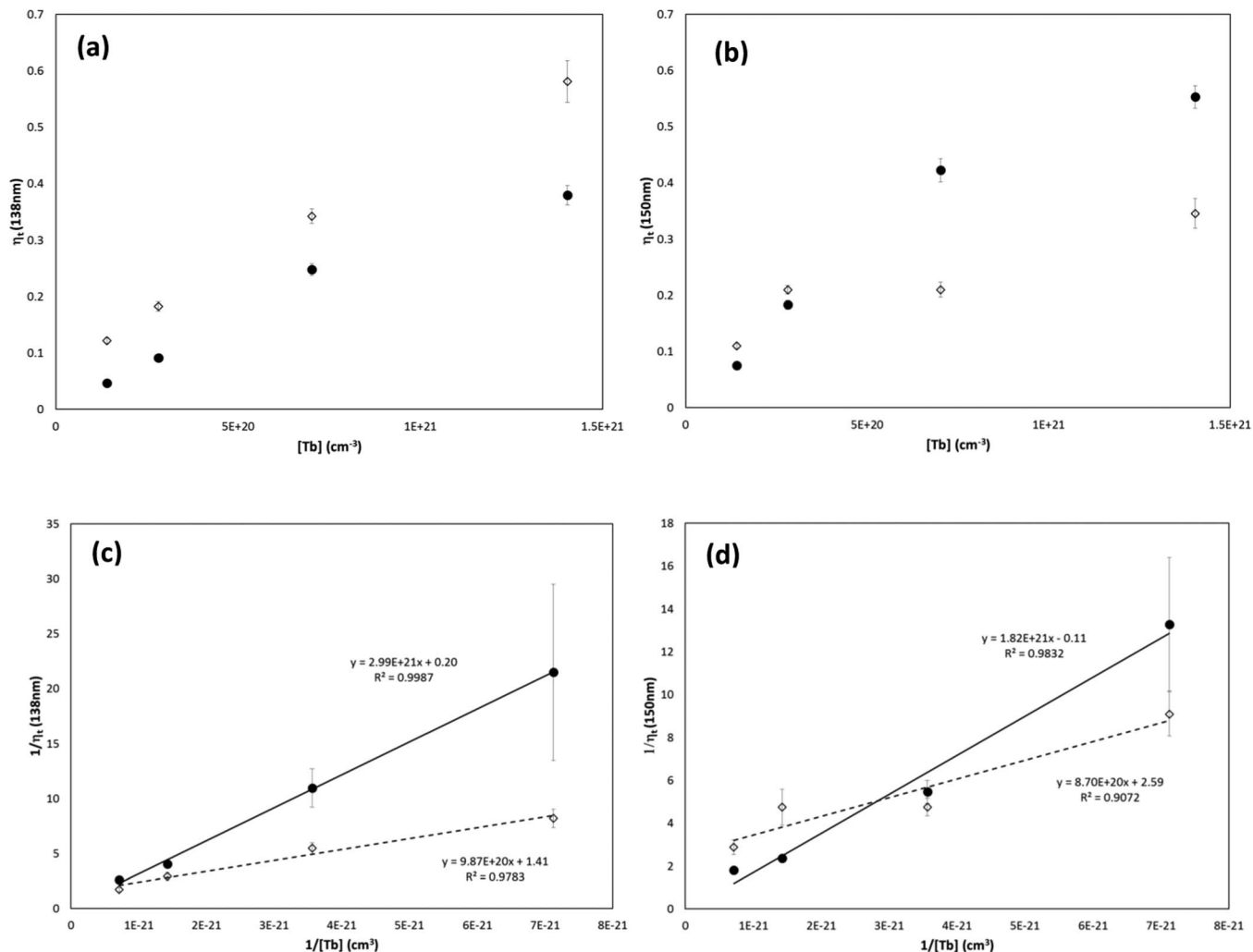


Figure 15. Transfer efficiency versus Tb^{3+} concentration in $\text{YPO}_4:\text{Tb}$ for excitation at (a) 138 nm and (b) 150 nm. Reciprocal plots of these data are in (c) and (d). Solid circles are for samples prepared by solid state reaction, while open diamonds were prepared via co-precipitation.

important to point out that this analysis does not allow us to distinguish loss to surface defect states from loss to an amorphous phase at the grain boundaries.

The surface or interface loss imposes a limit on the maximum value observed for η_t . This can clearly be seen when comparing 20 nm particles to 330 nm particles under 150 nm excitation in Figure 13b. The maximum transfer efficiency approaches 0.90 for 330 nm particles, but reaches a limit of about 0.30 in the 20 nm particles. Equation 4 can be rearranged to slope-intercept form as:

$$\frac{1}{\eta_t} = \frac{1}{S_{\text{loss}}} + \frac{\beta}{\alpha N} \left(\frac{1}{S_{\text{loss}}} \right) \quad [5]$$

where a plot of $1/\eta_t$ versus $1/N$ will have a slope of $\beta/(\alpha \cdot S_{\text{loss}})$ and a y-intercept of $1/S_{\text{loss}}$.

Such plots are shown in Figures 13–15, and the parameters calculated from linear regression are given in Tables I and II. The values of α and β cannot be extracted independently from these plots. However, the term α/β gives a relative assessment of the e-h pair mobility and capture efficiency for a given system, and allows us to quantify and compare some of our qualitative observations. As noted above, S_{loss} should have values between 0 and 1, which is generally observed in our data. However, the solid state Tb data yield unrealistic values. Here, we find $S_{\text{loss}} = 5.1$ and $S_{\text{loss}} = -9.1$ at 138 nm and 150 nm, respectively. We attribute this at least partly to the absorption data. Samples doped with Tb consistently produced noisier, lower quality reflectance

spectra. In addition, measured host absorption values decrease slightly with Tb concentration, a phenomenon that was also observed in our prior study of $\text{YBO}_3:\text{Tb}$.¹⁵ This results in an anomalously low value of $1/\eta_t$ and an unreasonable intercept. Because of this, we have also reported the α/β ratios obtained if S_{loss} isn't taken into account.

Higher α/β ratios imply more efficient trapping of the e-h pair by the dopant. From the data in the tables, it is clear that for Eu and Sm energy transfer is more efficient for excitation right at the band edge (150 nm) for both particle sizes, when compared with excitation at 138 nm. Excitation at 150 nm in the large particles is unusually

Table I. Kinetic parameters obtained from reciprocal plots for excitation at 138 nm. SS = solid state preparation; CP = co-precipitation. The number in parentheses for Tb is the α/β ratio calculated if S_{loss} is ignored, given the physically unrealistic values calculated from the intercept.

Ln^{3+}	Synthesis	α/β (cm^3)($\times 10^{21}$)	S_{loss}
Sm	SS	$1.84 \pm .11$	$0.76 \pm .10$
	CP	$4.39 \pm .46$	$0.66 \pm .06$
Eu	SS	$2.09 \pm .04$	$0.65 \pm .03$
	CP	$1.79 \pm .11$	$0.61 \pm .09$
Tb	SS	$0.065 \pm .002$ ($0.33 \pm .01$)	5.1 ± 8.1
	CP	$1.42 \pm .15$	$0.71 \pm .21$

Table II. Kinetic parameters obtained from reciprocal plots for excitation at 150 nm. SS = solid state preparation; CP = co-precipitation. The number in parentheses for Tb is the α/β ratio calculated if S_{loss} is ignored, given the physically unrealistic values calculated from the intercept.

Ln ³⁺	Synthesis	α/β (cm ³)($\times 10^{21}$)	S_{loss}
Sm	SS	14.1 \pm 4.3	0.73 \pm .06
	CP	4.03 \pm .65	0.31 \pm .05
Eu	SS	11.5 \pm 1.3	0.94 \pm .03
	CP	1.81 \pm .26	0.42 \pm .14
Tb	SS	0.060 \pm .006 (0.55 \pm .05)	-9.1 \pm 58.6
	CP	2.98 \pm .67	0.39 \pm 0.12

efficient, consistent with the intense peak in the excitation spectra. The efficiency of trapping by Tb³⁺ appears to be much less sensitive to the excitation wavelength, and is generally a factor of at least 10 lower than is observed for Eu³⁺ and Sm³⁺ in the samples prepared by solid state methods. The efficiency of trapping under 138 nm excitation appears to be less sensitive to the preparation method for all dopants.

In a previous comprehensive study of doped YBO₃, α/β ratios ($\times 10^{21}$ in units of cm³ as in Tables I and II) for Eu³⁺, Sm³⁺ and Tb³⁺ were found to be 7.7, 4.1, and 1.21, respectively. In the YBO₃ study it was argued that dopants with ground states in the valence band and Ln²⁺ ground states in the bandgap will act as electron traps, forming a charge transfer trap state (Ln²⁺ and a hole in the valence band), while dopants with ground state energies greater than the valence band will capture the e-h pair simultaneously (forming an excited state Ln³⁺).¹⁵ Electron traps generally exhibited more efficient trapping. The results for the three dopants studied here are consistent with those findings. Eu³⁺ and Sm³⁺ have ground states in or near the valence band, and α/β ratios of 14.1×10^{21} cm³ and 11.5×10^{21} cm³, while the Tb³⁺ ground state is nearly 3 eV above the valence band¹³ and has an α/β ratio of less than 1×10^{21} cm³ under 150 nm excitation. The same trend exists under 138 nm excitation, although the difference is less dramatic. We believe this is a significant finding, as it points to a potential means of predicting the trapping efficiency of doped materials from the energy level scheme.

A second, or perhaps supplementary explanation might be made regarding the different behavior of Tb³⁺ compared to Sm³⁺ and Eu³⁺ under 150 nm excitation. In the YPO₄:Ln³⁺ work of van Pieteron et al., they observe 4fⁿ⁻¹5d¹ states for Sm³⁺ and Eu³⁺ that extend very close to the STE excitation edge (147 nm and 153 nm for Sm³⁺, 152 nm for Eu³⁺).⁷ This may allow for resonant energy transfer between host STE and dopant energy levels. In the case of Tb³⁺, the dopant transitions are only observed down to 161 nm.⁸ Excitation at 138 nm, which involves the creation of a mobile e-h pair, does not provide for this resonant transfer mechanism.

At both excitation wavelengths, the effect of smaller particle size is seen as a smaller calculated value of S_{loss} . Recall that S_{loss} represents the fraction of e-h pairs available for trapping, and from our analysis it appears that under 150 nm excitation about twice as much energy is lost to surface or interface states in going from a particle size of 330 nm down to 20 nm (i.e., S_{loss} decreases by a factor of about 2). Our current interpretation of this result is that sample prepared by co-precipitation have an amorphous phase at the grain boundaries that absorbs the 150 nm excitation energy. However, we cannot discount the possibility that the loss is due to surface states. Our primary reason for assigning the loss to an amorphous phase is the absorption data that show the long absorption tail beyond the band edge in co-precipitation samples. This phase does not appear to interfere with excitation at 138 nm, where the values of S_{loss} are around 0.6 and are relatively insensitive to the preparation method.

Conclusions

We have evaluated the optical properties of YPO₄:Ln³⁺ (Ln = Eu, Sm, or Tb) prepared by co-precipitation and by solid state grinding and firing. Co-precipitation yields crystallite sizes of about 20 nm, while crystallites prepared by grinding and firing are about 330 nm. Excitation spectra of samples prepared by grinding and firing exhibit an unusually intense peak at 150 nm, which corresponds to formation of an STE in the host. We note a possible correlation between the intensity of this peak and the location of the Ln³⁺ ground state relative to YPO₄ valence and conduction bands, as well as a correlation with 4fⁿ⁻¹5d¹ energies calculated in prior publications. The peak at 150 nm decreases dramatically in samples prepared by co-precipitation. We suspect that this is due to the presence of an amorphous phase at the grain boundaries of materials prepared by co-precipitation, although it could also be due to surface defect states.

Using excitation and reflectance spectra, host-to-activator transfer efficiencies were calculated and modeled using first order competition kinetics. From this, we find that trapping efficiencies are especially high for excitation at the band edge in samples prepared by solid state reaction. At the band edge, Sm³⁺ and Eu³⁺ exhibit α/β ratios at least 10 times greater than Tb³⁺ in samples prepared by grinding and firing. The α/β ratio is calculated from fits to the model and is an indicator of e-h pair trapping efficiency. The difference in efficiencies among dopants may also be correlated with the energy level scheme, as was observed in YBO₃. The trapping efficiency decreases substantially in the smaller particles. Trapping efficiencies under 138 nm excitation, which corresponds to the formation of an e-h pair, are relatively insensitive to the preparation method.

For excitation at 150 nm, the kinetic analysis indicates that about 60% of e-h pairs are lost to the surface in the 20 nm material, while this number is 10–30% in the 330 nm material. This number is 30–40% under 138 nm excitation regardless of the preparation method.

Acknowledgments

Funding for this research was provided by the National Science Foundation Division of Materials Research (#1307092) and the CWU Office of Graduate Studies and Research.

References

1. A. K. Parchur and R. S. Ningthoujam, *RSC Advances*, **2**, 10859 (2012)
2. W. Jia, Y. Zhou, D. A. Keszler, J.-Y. Jeong, K. W. Jang, and R. S. Meltzer, *Phys. Stat. Sol. C*, **48** (2005).
3. E. Nakazawa and F. Shiga, *J. Lumin.*, **15**, 255 (1977).
4. E. Nakazawa, *J. Lumin.*, **100**, 89 (2002).
5. H. Lai, H. Yang, C. Tao, and X. Yang, *Phys. Stat. Sol. A*, **204**, 1178 (2007).
6. W. Di, X. Wang, B. Chen, H. Lai, and X. Zhao, *Opt. Mat.*, **27**, 1386 (2005).
7. L. van Pieteron, M. F. Reid, R. T. Wegh, S. Soverna, and A. Meijerink, *Phys. Rev. B*, **65**, 045113 (2002).
8. L. van Pieteron, M. F. Reid, R. T. Wegh, S. Soverna, and A. Meijerink, *Phys. Rev. B*, **65**, 045114 (2002).
9. V. N. Makhov, N. Yu. Kirikova, M. Kirm, J. C. Krupa, P. Liblik, A. Lushchik, Ch. Lushchik, E. Negodin, and G. Zimmerer, *Nuc. Inst. Meth. Phys. Res. A*, **486**, 437 (2002).
10. T. Grzyb, A. Gruszczyka, and S. Lis, *J. Lumin.*, **175**, 21 (2016).
11. A. J. J. Bos, N. R. J. Poolton, J. Wallinga, A. Bessière, and P. Dorenbos, *Rad. Meas.*, **45**, 343 (2010).
12. P. Dorenbos, A. J. J. Bos, and N. R. J. Poolton, *Opt. Mat.*, **33**, 1019 (2011).
13. A. J. J. Bos, P. Dorenbos, A. Bessière, and B. Viana, *Rad. Meas.*, **43**, 222 (2008).
14. P. Dorenbos and A. J. J. Bos, *Rad. Meas.*, **43**, 139 (2008).
15. M. K. Wallace and A. L. Diaz, *J. Lumin.*, **161**, 403 (2015).
16. K. Olsen, A. Lawler, and A. L. Diaz, *J. Phys. Chem. C*, **115**, 17136 (2011).
17. C. Waite, R. Mann, and A. L. Diaz, *J. Solid State Chem.*, **198**, 357 (2013).
18. W. O. Milligan, D. F. Mullica, G. W. Beall, and L. A. Boatner, *Inorg. Chimica Acta*, **60**, 39 (1982).
19. D. Wang, S. Xia, and Y. Min, *J. Rare Earths*, **26**, 439 (2008).
20. R. Rabinovitz, K. Johnston, and A. L. Diaz, *J. Phys. Chem. C*, **114**, 13884 (2010).
21. T. Watrous-Kelly, A. L. Diaz, and T. A. Dang, *Chem. Mater.*, **18**, 3130 (2006).
22. P. Dorenbos, *J. Lumin.*, **111**, 89 (2005).
23. K. C. Mishra and M. Raukas, *J. Electrochem. Soc.*, **151**, H105 (2004).